Int. J. Heat Mass Transfer. Vol. 35, No. 8, pp. 1913–1925, 1992
Printed in Great Britain

0017-9310/92 $5.00+0.00

Nonparallel thermal instability of mixed convection flow on nonisothermal horizontal and inclined flat plates

H. R. LEE, T. S. CHEN and B. F. ARMALY

Department of Mechanical and Aerospace Engineering and Engineering Mechanics, University of Missouri–Rolla, Rolla, MO 65401, U.S.A.

(*Received* 22 *January* 1991 *and in final form* 17 *July* 1991)

Abstract—A linear theory based on the nonparallel flow model is employed to study the onset of longitudinal vortex instability of laminar mixed convection flow over horizontal and inclined flat plates with variable surface temperature, $T_w(x)-T_\infty = Ax^n$. In the analysis, the streamwise dependence of the disturbance amplitude functions is taken into account. Neutral stability curves as well as the critical values for the parameter $G^* = Gr_x^*/Re_x^{*3/2}$ and wave number α^* are presented for Prandtl numbers $Pr = 0.7$, 7, 100, and 1000 over a range of the exponent values $-0.5 \leqslant n \leqslant 1.0$ and inclination angles $0° \leqslant \phi \leqslant 85°$. For a given Prandtl number and inclination angle, thermal instability is found to decrease as the value of the exponent n increases. Also, for given values of the exponent n and Prandtl number Pr, the critical value of $Gr_x^*/Re_x^{*3/2}$ increases with increasing inclination angle from the horizontal. However, the critical wave number α^* appears to be unaffected by the inclination angle. The results from the present nonparallel flow analysis are compared with available analytical and experimental results from previous studies. The nonparallel flow analysis that accounts for the streamwise dependence of the amplitude functions is found to have a stabilizing effect as compared with the parallel flow analysis in which the streamwise dependence of the disturbance is neglected.

INTRODUCTION

THE INSTABILITY of laminar mixed convection flows, which may arise in the form of Tollmien–Schlichting waves or longitudinal vortex rolls, has been the subject of many studies. The longitudinal vortex mode of instability arises when a fluid layer heated from below or cooled from above induces a buoyancy force component that is normal to the surface. This situation is analogous to the occurrence of Goertler vortices in boundary-layer flow along a concave wall which are induced by a centrifugal force normal to the wall. Thus, vortex rolls on a heated flat plate are induced by the buoyancy force, whereas those on a concave wall are caused by the centrifugal force.

In almost all of the analytical studies on vortex instability of laminar forced or mixed convection flow (see, for example, refs. [1–3]), a linear parallel flow model is employed, in which the disturbances are assumed to be independent of the streamwise direction. This approximate analysis has provided critical values of $Gr_x^*/Re_x^{*3/2}$ that are about two to three orders of magnitude lower than those observed in experiments (see, for example, refs. [4–9]). There is evidence from recent studies on the vortex instability of forced convection flow [10–12] and the vortex instability of natural convection flow over horizontal and inclined flat plates [13, 14] to indicate that the nonparallel flow analysis will yield more realistic predictions of the instability characteristics, when compared with experimental data, than the parallel flow analysis. This has motivated the present study.

In this study, vortex instability of laminar mixed convection flow over upward-facing, heated horizontal and inclined flat plates, with an acute angle ϕ from the horizontal, is examined for the situation in which the surfaced temperature of the plate varies with the axial distance x as $T_w(x)-T_\infty = Ax^n$. The analysis is based on the linear theory using a nonparallel flow model. The resulting eigenvalue problem for the disturbance amplitude functions was solved by an efficient finite-difference method [15] in conjunction with Müller's shooting procedure.

Main-flow characteristics, neutral stability curves as well as the critical values of $Gr_x^*/Re_x^{*3/2}$ and wave number were obtained over a range of inclination angles $0° \leqslant \phi \leqslant 85°$, Prandtl numbers $0.7 \leqslant Pr \leqslant 1000$, and the exponent values $-0.5 \leqslant n \leqslant 1.0$.

ANALYSIS

The main-flow and thermal fields

Attention is first directed to the main-flow and thermal fields. Consider laminar mixed convection flow over horizontal and inclined heated flat plates with the surface temperature varying as $T_w(x) = T_\infty + Ax^n$, where A and n are real constants and T_∞ is the free stream temperature. The angle of inclination from the horizontal is ϕ. Let U_∞ be the free stream velocity, and let the streamwise and normal coordinates be x and y, with the corresponding velocity components U and V. The governing boundary-layer equations for constant-property fluids under the Boussinesq approximation can be written as [16]

NOMENCLATURE

a	dimensionless azimuthal wave number of disturbances
C_{f_x}	local friction factor, $\tau_w/(\rho U_\infty^2/2)$
D	partial derivative with respect to η
f	reduced stream function, $\psi/(\nu U_\infty x)^{1/2}$
g	gravitational acceleration
Gr_x	local Grashof number, $g\beta[T_w(x)-T_\infty]x^3/\nu^2$
Gr_L	Grashof number based on L, $g\beta[T_w(L)-T_\infty]L^3/\nu^2$
h	local heat transfer coefficient
k	thermal conductivity
L	characteristic length
n	exponent in the power-law variation of the wall temperature
Nu_x	local Nusselt number, hx/k
p'	perturbation pressure
P	main-flow pressure
Pr	Prandtl number
Re_x	local Reynolds number, $U_\infty x/\nu$
Re_L	Reynolds number based on L, $U_\infty L/\nu$
t	dimensionless amplitude function of temperature disturbance
t'	perturbation temperature
T	main-flow temperature
u, v, w	dimensionless amplitude functions of velocity disturbance in the x, y, z directions, respectively
u', v', w'	streamwise, normal, and spanwise components of perturbation velocity
U, V	streamwise and normal velocity components of main flow in the x, y directions, respectively
x, y, z	streamwise, normal, and spanwise coordinates
X, Y, Z	dimensionless streamwise, normal, and spanwise coordinates, defined, respectively, as x/L, $y/(\varepsilon L)$, $z/(\varepsilon L)$.

Greek symbols

α	dimensionless wave number of disturbances, $aX^{1/2}$
β	volumetric coefficient of thermal expansion
δ	boundary layer thickness
ε	dimensionless parameter, defined as $Re_L^{-1/2}$
η	pseudo-similarity variable, $y(U_\infty/\nu x)^{1/2}$
θ	dimensionless temperature, $(T-T_\infty)/[T_w(x)-T_\infty]$
κ	thermal diffusivity of fluid
ν	kinematic viscosity of fluid
ξ	buoyancy force parameter, $\lvert Gr_x\rvert/Re_x^2$
ρ	density of fluid
τ_w	local wall shear stress
ϕ	angle of inclination from the horizontal
ψ	stream function.

Superscripts

$+$	dimensionless disturbance quantity
$-$	scale quantity defined by equation (32)
$*$	critical condition or dimensionless main flow quantity
$\wedge$	resultant quantity.

Subscripts

o	dimensionless amplitude function
w	condition at wall
∞	condition at free stream.

$$\frac{\partial U}{\partial x}+\frac{\partial V}{\partial y}=0 \tag{1}$$

$$U\frac{\partial U}{\partial x}+V\frac{\partial U}{\partial y}=\pm g\beta\cos\phi\,\frac{\partial}{\partial x}\int_y^\infty (T-T_\infty)\,\mathrm{d}y \pm g\beta(T-T_\infty)\sin\phi+\nu\frac{\partial^2 U}{\partial y^2} \tag{2}$$

$$U\frac{\partial T}{\partial x}+V\frac{\partial T}{\partial y}=\kappa\frac{\partial^2 T}{\partial y^2}. \tag{3}$$

The corresponding boundary conditions are

$$\begin{aligned} &U=V=0 \quad T=T_w(x)=T_\infty+Ax^n \quad \text{at} \quad y=0\\ &U\to U_\infty \quad T\to T_\infty \quad \text{as} \quad Y\to\infty\\ &U=U_\infty \quad T=T_\infty \quad \text{at} \quad x=0. \end{aligned} \tag{4}$$

The first term on the right-hand side of equation (2) represents the buoyancy-induced streamwise pressure gradient, with the plus and minus signs pertaining to flows above and below the plate, respectively. The second term on the right-hand side of the same equation denotes the streamwise component of the buoyancy force, and the plus and minus signs refer, respectively, to upward and downward flows. Furthermore, equation (2) can be reduced to that for a horizontal plate without the streamwise component of the buoyancy force term when $\phi = 0°$ and to that for a vertical plate without the buoyancy-induced streamwise pressure gradient term when $\phi = 90°$.

Next, the system of equations (1)–(4) can be transformed into a dimensionless form as

$$f'''+\tfrac{1}{2}ff''\pm\xi\theta\sin\phi \pm\xi\,Re_x^{-1/2}\cos\phi\left[\frac{1}{2}\eta\theta+(\tfrac{1}{2}+n)\int_\eta^\infty\theta\,\mathrm{d}\eta +(n+1)\xi\int_\eta^\infty\frac{\partial\theta}{\partial\xi}\,\mathrm{d}\eta\right]=(n+1)\xi\left[f'\frac{\partial f'}{\partial\xi}-f''\frac{\partial f}{\partial\xi}\right] \tag{5}$$

$$\theta''+\tfrac{1}{2}Pr\,f\theta'-n\,Pr\,f'\theta = (n+1)\,Pr\,\xi\left[f'\frac{\partial\theta}{\partial\xi}-\theta'\frac{\partial f}{\partial\xi}\right] \quad (6)$$

$$f(\xi,0)=f'(\xi,0)=0,\quad f'(\xi,\infty)=1$$
$$\theta(\xi,0)=1,\quad \theta(\xi,\infty)=0 \quad (7)$$

where the pseudo-similarity variable $\eta(x,y)$, the reduced stream function $f(\xi,\eta)$, the dimensionless temperature $\theta(\xi,\eta)$, the buoyancy force parameter $\xi(x)$, the local Reynolds number Re_x, and the local Grashof number Gr_x are as defined in the Nomenclature. In equations (5)–(7), the primes denote partial derivatives with respect to η and Pr is the Prandtl number. It is noted here that $\xi(x)$ measures the magnitude of the buoyancy force effect and the plus and minus signs that appear on the left-hand side of equation (5) now pertain to assisting and opposing flows, respectively.

From an order-of-magnitude analysis, it has been demonstrated [16] that in equation (5) the buoyancy-induced streamwise pressure gradient term can be neglected in comparison with the buoyancy force component term if the condition

$$\eta_\infty/Re_x^{1/2} \ll \tan\phi \quad (8)$$

prevails. This condition was shown to provide accurate main-flow results for $15^\circ \leqslant \phi \leqslant 90^\circ$ for all practical purposes for η_∞ (the dimensionless boundary-layer thickness) of about 10 and $Re_x \geqslant 10^3$ [16]. Within the framework of the condition (8), equation (5) can be reduced to

$$f'''+\tfrac{1}{2}ff''\pm\xi\theta\sin\phi = (n+1)\xi\left[f'\frac{\partial f'}{\partial\xi}-f''\frac{\partial f}{\partial\xi}\right] \quad (9)$$

for $15^\circ \leqslant \phi \leqslant 90^\circ$.

On the other hand, the buoyancy force component term may be neglected in comparison with the buoyancy-induced streamwise pressure gradient term when the condition

$$\tan\phi \ll \eta_\infty/Re_x^{1/2} \quad (10)$$

holds true for $0^\circ \leqslant \phi \leqslant 15^\circ$. Under this condition, equation (5) can be reduced to

$$f'''+\tfrac{1}{2}ff''\pm\xi\,Re_x^{-1/2}\cos\phi\left[\frac{1}{2}\eta\theta+(\tfrac{1}{2}+n)\int_\eta^\infty\theta\,\mathrm{d}\eta + (n+1)\xi\int_\eta^\infty\frac{\partial\theta}{\partial\xi}\mathrm{d}\eta\right] = (n+1)\xi\left[f'\frac{\partial f'}{\partial\xi}-f''\frac{\partial f}{\partial\xi}\right]. \quad (11)$$

In addition, when $\xi\,Re_x^{-1/2} \ll 1$ and $\xi\partial/\partial\xi \ll 1$ for small values of ξ, equation (11) and equation (6) can be reduced to

$$f'''+\tfrac{1}{2}ff''=0 \quad (12)$$

$$\theta''+\tfrac{1}{2}Pr\,f\theta'-n\,Pr\,f'\theta=0. \quad (13)$$

The flow is most susceptible to the vortex mode of instability when $\phi = 0^\circ$. The results for $\phi = 0^\circ$ and $\xi = 0$ (pure forced convection) have been given in ref. [12].

The main-flow quantities of interest are the axial velocity profile $f'(\xi,\eta) = U/U_\infty$, the temperature profile $\theta(\xi,\eta)$, the local Nusselt number Nu_x, and the local friction factor C_{f_x}. In terms of the dimensionless variables, the last two quantities can be expressed, respectively, by

$$Nu_x\,Re_x^{-1/2} = -\theta'(\xi,0),$$
$$C_{f_x}Re_x^{1/2} = 2f''(\xi,0). \quad (14)$$

The case of uniform wall temperature (UWT) corresponds to $n = 0$.

Formulation of the stability problem

In the present analysis, a linear stability theory is employed. In experiments [4–9] the 'stationary' longitudinal vortex rolls have been found to be periodic in the spanwise direction z. Thus, the disturbance quantities for velocity components u', v', w', pressure p', and temperature t' are assumed to be functions of (x,y,z). These disturbance quantities are superimposed on the two-dimensional main-flow quantities U, V, $W = 0$, P, and T to obtain the resultant quantities $\hat{U}$, $\hat{V}$, $\hat{W}$, $\hat{P}$, and $\hat{T}$ as follows:

$$\hat{U}(x,y,z) = U(x,y)+u'(x,y,z)$$
$$\hat{V}(x,y,z) = V(x,y)+v'(x,y,z)$$
$$\hat{W}(x,y,z) = w'(x,y,z)$$
$$\hat{P}(x,y,z) = P(x,y)+p'(x,y,z)$$
$$\hat{T}(x,y,z) = T(x,y)+t'(x,y,z). \quad (15)$$

The resultant quantities given by equation (15) satisfy the continuity equation, the Navier–Stokes equations, and the energy equation for an incompressible, three-dimensional steady fluid flow. Substituting equation (15) into these equations, subtracting the two-dimensional main flow, and linearizing the disturbance quantities, one can arrive at the following disturbance equations:

$$\frac{\partial u'}{\partial x}+\frac{\partial v'}{\partial y}+\frac{\partial w'}{\partial z}=0 \quad (16)$$

$$u'\frac{\partial U}{\partial x}+U\frac{\partial u'}{\partial x}+v'\frac{\partial U}{\partial y}+V\frac{\partial u'}{\partial y} = -\frac{1}{\rho}\frac{\partial p'}{\partial x}+\nu\nabla^2u'+g\beta\sin\phi t' \quad (17)$$

$$u'\frac{\partial V}{\partial x}+U\frac{\partial v'}{\partial x}+v'\frac{\partial V}{\partial y}+V\frac{\partial v'}{\partial y} = -\frac{1}{\rho}\frac{\partial p'}{\partial y}+\nu\nabla^2v'+g\beta\cos\phi t' \quad (18)$$

$$U\frac{\partial w'}{\partial x}+V\frac{\partial w'}{\partial y}=-\frac{1}{\rho}\frac{\partial p'}{\partial z}+\nu\nabla^2 w' \quad (19)$$

$$u'\frac{\partial T}{\partial x}+U\frac{\partial t'}{\partial x}+v'\frac{\partial T}{\partial y}+V\frac{\partial t'}{\partial y}=\kappa\nabla^2 t' \quad (20)$$

where $\nabla^2=\partial^2/\partial x^2+\partial^2/\partial y^2+\partial^2/\partial z^2$ is the Laplacian operator.

The analysis to follow is parallel to that described in ref. [12], and some details are omitted. Because the disturbances are confined within the boundary layer of the main flow, the so-called bottling effect [17], they will have length scales different from those of the main-flow field [18, 19]. To verify this, the disturbance equations are first nondimensionalized by using the length and velocity scales of the main flow

$$X=\frac{x}{L},\quad Y=\frac{y}{\varepsilon L},\quad Z=\frac{z}{\varepsilon L} \quad (21)$$

$$U^*=\frac{U}{U_\infty},\quad V^*=\frac{V}{\varepsilon U_\infty},\quad \theta=\frac{T-T_\infty}{T_w(x)-T_\infty} \quad (22)$$

where $\varepsilon=Re_L^{-1/2}$ and $Re_L=U_\infty L/\nu$ is the Reynolds number based on a characteristic length $L(x)$. If $L=x$, then $Y=\eta$ and $Re_L=Re_x$. It is noted that U^*, V^*, and θ and their derivatives with respect to X and Y are of the order of 1. Similarly, the disturbance quantities can be scaled as

$$u^+=\frac{u'}{U_\infty},\quad v^+=\frac{v'}{U_\infty},\quad w^+=\frac{w'}{U_\infty}$$

$$p^+=\frac{p'}{\rho U_\infty^2\varepsilon}=\frac{p'\,Re_L^{1/2}}{\rho U_\infty^2},\quad t^+=\frac{t'}{T_w(x)-T_\infty} \quad (23)$$

where u^+, v^+, w^+, p^+, and t^+ and their derivatives with respect to X and Y are of the order of ε.

Substitution of the dimensionless variables from equations (21)–(23) into equations (16)–(20) will give rise to a set of conservation equations for the disturbances that are identical to equations (15)–(19) in ref. [12], except that an additional term $(Gr_L/Re_L^2)\sin\phi t^+$ now appears on the right-hand side of the x-momentum equation and the term $(Gr_L/Re_L^2)t^+$ in the y-momentum equation is replaced with $(Gr_L/Re_L^2)\cos\phi t^+$. Here, $Gr_L=g\beta[T_w(L)-T_\infty]\times L^3/\nu^2$ is the Grashof number based on the characteristic length L. Furthermore, since Gr_L/Re_L^2 is of the order of 1 and Re_L is of the order of ε^{-2}, Gr_L is of the order of ε^{-4}. In these equations one will note that there is a term $(v^+/\varepsilon)\,\partial U^*/\partial Y$ in the x-momentum disturbance equation and a term $(v^+/\varepsilon)\times\partial\theta/\partial Y$ in the energy disturbance equation that are larger than other terms in the corresponding equation by at least an order of $(1/\varepsilon)$. This means that the (X,Y,Z) variables as defined in equation (21) are not the appropriate length scales for the disturbances. Thus, by rescaling the coordinates for disturbance quantities along with the disturbance pressure in the form

$$(\bar X,\bar Y,\bar Z,\bar p^+)=(X,Y,Z,p^+)\varepsilon^{-1/2} \quad (24)$$

one can arrive at a set of disturbance equations identical to equations (21)–(25) in ref. [12], except that now an additional term $\varepsilon(Gr_L/Re_L^2)\sin\phi t^+$ appears on the right-hand side of the x-momentum equation and the term $\varepsilon(Gr_L/Re_L^2)t^+$ in the y-momentum equation is replaced with $\varepsilon(Gr_L/Re_L^2)\cos\phi t^+$. In this last set of equations, one will find that the terms $\varepsilon\,\partial u^+/\partial\bar X$, $\varepsilon^2\partial\bar p^+/\partial\bar X$, $\varepsilon^2\partial^2u^+/\partial\bar X^2$, $\varepsilon^2\partial^2v^+/\partial\bar X^2$, $\varepsilon^2\partial^2w^+/\partial\bar X^2$, and $\varepsilon^2\partial^2t^+/\partial\bar X^2$ are smaller than the rest of the terms in their respective equations and thus these terms can be omitted. The omission of these lowest order terms in the disturbance equations is consistent with the level of approximation of the main flow. With the above-mentioned terms deleted and by making use of equation (24), the disturbance equations are reduced to

$$\frac{\partial v^+}{\partial Y}+\frac{\partial w^+}{\partial Z}=0 \quad (25)$$

$$u^+\frac{\partial U^*}{\partial X}+U^*\frac{\partial u^+}{\partial X}+Re_L^{1/2}v^+\frac{\partial U^*}{\partial Y}+V^*\frac{\partial u^+}{\partial Y}=\frac{\partial^2u^+}{\partial Y^2}+\frac{\partial^2u^+}{\partial Z^2}+\frac{Gr_L}{Re_L^2}\sin\phi t^+ \quad (26)$$

$$Re_L^{-1/2}u^+\frac{\partial V^*}{\partial X}+U^*\frac{\partial v^+}{\partial X}+v^+\frac{\partial V^*}{\partial Y}+V^*\frac{\partial v^+}{\partial Y}=-\frac{\partial p^+}{\partial Y}+\frac{\partial^2v^+}{\partial Y^2}+\frac{\partial^2v^+}{\partial Z^2}+\frac{Gr_L}{Re_L^2}\cos\phi t^+ \quad (27)$$

$$U^*\frac{\partial w^+}{\partial X}+V^*\frac{\partial w^+}{\partial Y}=-\frac{\partial p^+}{\partial Z}+\frac{\partial^2w^+}{\partial Y^2}+\frac{\partial^2w^+}{\partial Z^2} \quad (28)$$

$$u^+\frac{\partial\theta}{\partial X}+U^*\frac{\partial t^+}{\partial X}+Re_L^{1/2}v^+\frac{\partial\theta}{\partial Y}+V^*\frac{\partial t^+}{\partial Y}=\frac{1}{Pr}\left[\frac{\partial^2t^+}{\partial Y^2}+\frac{\partial^2t^+}{\partial Z^2}\right]. \quad (29)$$

Note that the main-flow quantities, such as U^*, $\partial U^*/\partial X$, $\partial U^*/\partial Y$, V^*, $\partial V^*/\partial X$, $\partial V^*/\partial Y$, $\partial\theta/\partial X$, and $\partial\theta/\partial Y$ can be expressed in terms of $f(\xi,\eta)$, $\theta(\xi,\eta)$ and their ξ and η derivatives. For example, $U^*=f'(\xi,\eta)$, $V^*=-X^{-1/2}[f(\xi,\eta)-\eta f'(\xi,\eta)+2\xi\,\partial f/\partial\xi]/2$, and $\partial\theta/\partial Y=X^{-1/2}\theta'(\xi,\eta)$.

Next, the pressure terms in equations (27) and (28) are eliminated by cross-differentiation and subtraction. To remove the terms involving the function w^+ and its derivatives, the resulting equation is then differentiated with respect to Z once and the substitution $\partial w^+/\partial Z=-\partial v^+/\partial Y$ from the continuity equation is employed. This operation will yield three equations for the disturbance quantities u^+, v^+, and t^+. For the nonparallel flow model considered here, these quantities are expressed as

$$(u^+,v^+,t^+)=[u_o(X,Y),v_o(X,Y),t_o(X,Y)]\exp(iaZ) \quad (30)$$

where a is the dimensionless azimuthal wave number of the disturbances. That is, based on experimental observations, the longitudinal vortex rolls are taken to be periodic in the spanwise Z-direction, with the amplitude functions depending on both X and Y.

Next, substituting equation (30) into equation (26), the combined form of equations (27) and (28) as described above, and equation (29), along with the introduction of the coordinate transformation from (X, Y) to (X, η) through the relationship

$$Y = X^{1/2}\eta, \quad \frac{\partial}{\partial Y} = X^{-1/2}\frac{\partial}{\partial \eta}$$
$$Y\frac{\partial}{\partial Y} = Y\frac{\partial}{\partial \eta}\frac{\partial \eta}{\partial Y} = \eta\frac{\partial}{\partial \eta} \tag{31}$$

and letting

$$\alpha^2 = a^2 X, \quad u = u_o, \quad v = v_o Re_x^{1/2}, \quad t = t_0 \tag{32}$$

one can obtain the following system of partial differential equations for the disturbance amplitude functions u, v, and t

$$D^2u + a_1^* Du + a_2^* u + a_3^* v + a_4^* t = f' X\frac{\partial u}{\partial X} \tag{33}$$

$$D^4 v + b_1^* D^3 v + b_2^* D^2 v + b_3^* Dv + b_4^* v + b_5^* u + b_6^* t = f' X\frac{\partial}{\partial X}(D^2 v) + f'' X\frac{\partial}{\partial X}(Dv) - \alpha^2 f' X\frac{\partial v}{\partial X} \tag{34}$$

$$D^2 t + d_1^* Dt + d_2^* t + d_3^* u + d_4^* v = Pr\, f' X\frac{\partial t}{\partial X}, \tag{35}$$

with the boundary conditions

$$u = v = Dv = t = 0 \quad \text{at} \quad \eta = 0 \quad \text{and} \quad \eta = \infty. \tag{36}$$

In equations (33)–(35), the coefficients are given by

$$a_1^* = \frac{1}{2}\left(f - \eta f' + 2\xi\frac{\partial f}{\partial \xi}\right)$$
$$a_2^* = \frac{1}{2}\left(\eta f'' - 2\xi\frac{\partial f'}{\partial \xi}\right) - \alpha^2$$
$$a_3^* = -f'', \quad a_4^* = \xi \sin\phi$$
$$b_1^* = \frac{1}{2}\left(f - \eta f' + 2\xi\frac{\partial f}{\partial \xi}\right)$$
$$b_2^* = \tfrac{3}{2}f' - \tfrac{1}{2}\eta f'' - 2\alpha^2 + \xi\frac{\partial f'}{\partial \xi}$$
$$b_3^* = f''' - \tfrac{1}{2}\alpha^2\left(f - \eta f' + 2\xi\frac{\partial f}{\partial \xi}\right)$$
$$b_4^* = \alpha^4 + \tfrac{1}{2}\alpha^2\left(\eta f'' - f' - 2\xi\frac{\partial f'}{\partial \xi}\right)$$
$$b_5^* = \tfrac{1}{4}\alpha^2\left(f - \eta f' - \eta^2 f'' - 4\xi\frac{\partial f}{\partial \xi} + 4\eta\xi\frac{\partial f'}{\partial \xi} - 4\xi^2\frac{\partial^2 f}{\partial \xi^2}\right)$$
$$b_6^* = -\alpha^2(Gr_x/Re_x^{3/2})\cos\phi = -\alpha^2\xi\, Re_x^{1/2}\cos\phi$$
$$d_1^* = \tfrac{1}{2}Pr\left(f - \eta f' + 2\xi\frac{\partial f'}{\partial \xi}\right), \quad d_2^* = -\alpha^2$$
$$d_3^* = \tfrac{1}{2}Pr\left(\eta\theta' - 2\xi\frac{\partial \theta}{\partial \xi}\right), \quad d_4^* = -Pr\,\theta' \tag{37}$$

in which f and θ and their derivatives with respect to ξ and η are obtained from the main-flow solutions of equations (9), (6) and (7). Also, in equations (33)–(36), D^k stands for the kth partial derivative with respect to η. The boundary conditions (36) arise from the vanishing of the disturbances at the wall and in the free stream. The condition $Dv = 0$ results from the continuity equation (25) along with $w = 0$ at $\eta = 0$ and $\eta = \infty$.

As the main-flow and thermal fields are functions of (ξ, η), it is convenient to express the disturbance amplitude functions u, v, and t also as the functions of (ξ, η). From the $\xi(X)$ relationship one has

$$X\frac{\partial}{\partial X} = X\frac{\partial}{\partial \xi}\frac{d\xi}{dX} + X\frac{\partial}{\partial \eta}\frac{\partial \eta}{\partial X} = \xi\frac{\partial}{\partial \xi} - \tfrac{1}{2}\eta\frac{\partial}{\partial \eta}. \tag{38}$$

In terms of (ξ, η), equations (33)–(35) reduce to

$$D^2 u + a_1 Du + a_2 u + a_3 v + a_4 t = f'\xi\frac{\partial u}{\partial \xi} \tag{39}$$

$$D^4 v + b_1 D^3 v + b_2 D^2 v + b_3 Dv + b_4 v + b_5 u + b_6 t = f'\xi\frac{\partial}{\partial \xi}(D^2 v) + f''\xi\frac{\partial}{\partial \xi}(Dv) - \alpha^2 f'\xi\frac{\partial v}{\partial \xi} \tag{40}$$

$$D^2 t + d_1 Dt + d_2 t + d_3 u + d_4 v = Pr\, f'\xi\frac{\partial t}{\partial \xi} \tag{41}$$

along with boundary conditions as given by equation (36). The coefficients in equations (39)–(41) are defined by

$$a_1 = a_1^* + \tfrac{1}{2}\eta f', \quad a_2 = a_2^*, \quad a_3 = a_3^*, \quad a_4 = a_4^*$$
$$b_1 = b_1^* + \tfrac{1}{2}\eta f', \quad b_2 = b_2^* + \tfrac{1}{2}\eta f''$$
$$b_3 = b_3^* - \tfrac{1}{2}\alpha^2\eta f', \quad b_4 = b_4^*, \quad b_5 = b_5^*, \quad b_6 = b_6^*$$
$$d_1 = d_1^* + \tfrac{1}{2}Pr\,\eta f', \quad d_2 = d_2^*, \quad d_3 = d_3^*, \quad d_4 = d_4^*. \tag{42}$$

Equations (39)–(41), along with the boundary conditions (36), represent the mathematical system for the stability problem. Since equations (39)–(41) are partial differential equations, the boundary conditions as given by equation (36) are not sufficient if ξ derivatives of u, v, and t are not set equal to zero.

As the instability occurs at small ξ values, a simple approach to solve equations (39)–(41) with good approximation is to use the local similarity method by neglecting or truncating the terms involving $\partial u/\partial \xi$, $\partial v/\partial \xi$, and $\partial t/\partial \xi$ on the right-hand side of these equations. This will result in a system of homogeneous 'ordinary differential equations' for the disturbance amplitude functions u, v, and t as represented by equations (39)–(41) with their right-hand side terms deleted, along with the boundary conditions (36). This system of equations constitutes an eigenvalue problem of the form

$$E(\alpha, Re_x^{1/2}; Pr, n, \phi, \xi) = 0. \tag{43}$$

For given values of the buoyancy force parameter $\xi = Gr_x/Re_x^2$, inclination angle ϕ, exponent n, and Prandtl number Pr, the value of $Re_x^{1/2}$ satisfying equation (43) is sought as the eigenvalue for a prescribed value of the wave number α.

It is noted here that in the instability calculations for $0° \leqslant \phi \leqslant 15°$, the main-flow and thermal fields were obtained from equations (12) and (13), rather than from equations (11) and (6), subject to boundary conditions (7). This is because the flow instability occurs at very small values of ξ and equations (11) and (6) reduce to equations (12) and (13) when $\xi \ll 1$.

NUMERICAL METHOD OF SOLUTION

The system of equations for the main-flow and thermal fields, equations (9), (6), and (7) for $15° \leqslant \phi \leqslant 90°$, was solved by a finite-difference scheme in conjunction with a cubic spline interpolation method similar to, but modified from, that described in ref. [15] to provide the main-flow quantities f, f', f'', θ, and θ' that are needed in the stability computation as well as in the determination of the local Nusselt number and the local friction factor. To conserve space, the details of the finite-difference method of solution are omitted here. The stability problem, described by equations (39)–(41) with their right-hand side terms deleted and the boundary conditions given by equation (36), was solved by a finite-difference scheme along with Müller's shooting method. This solution method parallels that described in ref. [15] and no details need to be given here. Equations (6) and (41) will become stiff when the Prandtl number is large. To solve stiff differential equations by the finite-difference method, an upwind scheme or its equivalent is required. In the present study, a finite-difference method based on a weighting factor [15] is used, which enables the numerical scheme to shift automatically from the central difference algorithm to the upwind difference algorithm, and vice-versa. To proceed with numerical calculations of the stability problem, the boundary conditions at $\eta = \eta_\infty$ are first approximated by the asymptotic solutions of the truncated equations (39)–(41) at $\eta = \eta_\infty$ (i.e. at the edge of the boundary layer). Since $f'' = \theta = \theta' = 0$ at $\eta = \eta_\infty$, the asymptotic solutions for u, v, and t at $\eta = \eta_\infty$ can be obtained as

$$\begin{gathered} u_2 = \exp(-m\eta_\infty), \quad u_3 = \exp(-r\eta_\infty) \\ u_1 = u_4 = 0, \quad v_1 = \exp(-\alpha\eta_\infty) \\ v_2 = \exp(-m\eta_\infty), \quad v_3 = \exp(-r\eta_\infty) \\ v_4 = \exp(-b\eta_\infty), \quad t_3 = \exp(-r\eta_\infty) \\ t_1 = t_2 = t_4 = 0 \end{gathered} \tag{44}$$

where

$$\begin{aligned} r &= \{-Pr\,C_1 + [(Pr\,C_1)^2 + 4\alpha^2]^{1/2}\}/2 \\ m &= \{-C_1 + [C_1^2 + 4\alpha^2]^{1/2}\}/2 \\ b &= \{-C_1 + [C_1^2 + 4(\alpha^2 - f'/2)]^{1/2}\}/2 \end{aligned} \tag{45}$$

with $C_1 = -(f + 2\xi\,\partial f/\partial \xi)/2$. At any η location, the solutions for u, v, and t can be represented by

$$\begin{aligned} u(\xi,\eta) &= K_1 u_1(\xi,\eta) + K_2 u_2(\xi,\eta) \\ &\quad + K_3 u_3(\xi,\eta) + K_4 u_4(\xi,\eta) \\ v(\xi,\eta) &= K_1 v_1(\xi,\eta) + K_2 v_2(\xi,\eta) \\ &\quad + K_3 v_3(\xi,\eta) + K_4 v_4(\xi,\eta) \\ t(\xi,\eta) &= K_1 t_1(\xi,\eta) + K_2 t_2(\xi,\eta) \\ &\quad + K_3 t_3(\xi,\eta) + K_4 t_4(\xi,\eta) \end{aligned} \tag{46}$$

where K_1, K_2, K_3, and K_4 are constants.

With preassigned values of the buoyancy parameter ξ, inclination angle ϕ, and exponent n, the main-flow solution is first obtained for a fixed Prandtl number, Pr. Next, with the wave number α specified and the estimated value of $Re_x^{1/2}$, the finite-difference form of the truncated equations (39)–(41), along with boundary conditions (36), is numerically solved from $\eta = 0$ to $\eta = \eta_\infty$, ending with the asymptotic solutions for u, v, and t at $\eta = \eta_\infty$. The correction for the value of $Re_x^{1/2}$ is then made by Müller's shooting method until the boundary conditions at the wall are satisfied within a tolerance of less than 10^{-6}. This yields a converged value of $Re_x^{1/2}$ as the eigenvalue for given values of ξ, ϕ, n, Pr and α.

After some numerical experiments, a step size of $\Delta\eta = 0.005$ and a value of $\eta_\infty = 10$ were found to be sufficient for both the main-flow and the stability calculations for all inclination angles, $15° \leqslant \phi \leqslant 90°$, exponent values $-0.5 \leqslant n \leqslant 1.0$ and $Pr = 100$ and 1000. However, for the cases of $Pr = 0.7$ and 7, because of the relatively small critical wave numbers α^*, convergent solutions were difficult to obtain for the step size $\Delta\eta$ that was used. To cope with the numerical difficulties associated with smaller values of Prandtl number, Pr, say $Pr = 0.7$ and 7, results for these two Prandtl numbers were obtained for $\phi = 0$ and 85° from which an interpolation method was used to obtain the critical $Gr_x^*/Re_x^{*3/2}$ results for all angles of inclination.

RESULTS AND DISCUSSION

The local Nusselt number in terms of $Nu_x \times Re_x^{-1/2} = -\theta'(\xi, 0)$ and the local friction factor in terms of $C_{f_x} Re_x^{1/2}/2 = f''(\xi, 0)$ for $Pr = 0.7$, 7, 100, and 1000 were obtained. To illustrate the effects of the exponent n on the friction factor and the local Nusselt number, Figs. 1, 2, 3 and 4 have been prepared for two

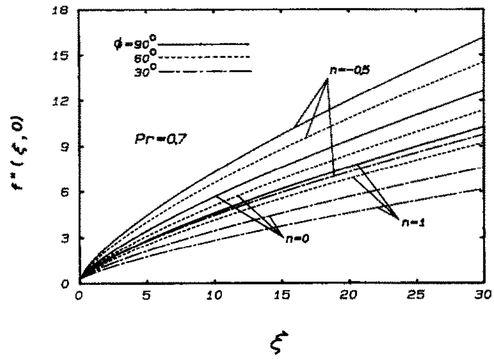

FIG. 1. Local friction factor, $Pr = 0.7$.

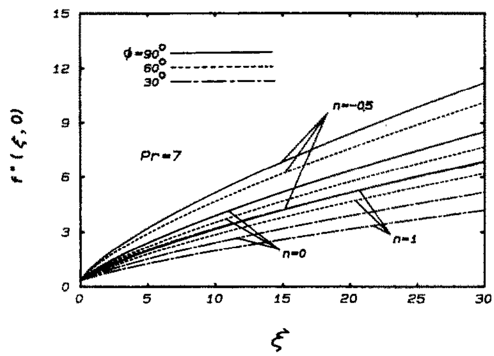

FIG. 2. Local friction factor, $Pr = 7$.

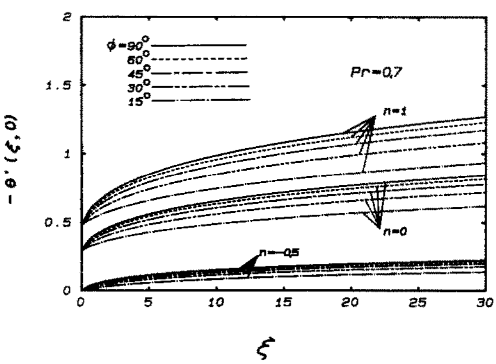

FIG. 3. Local Nusselt number, $Pr = 0.7$.

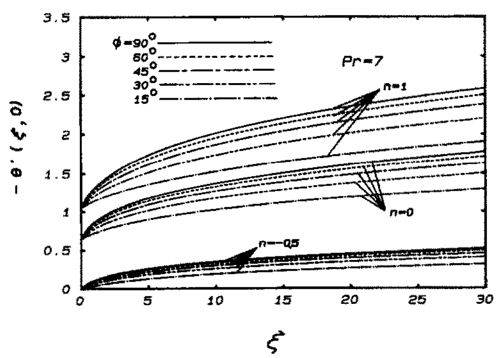

FIG. 4. Local Nusselt number, $Pr = 7$.

representative Prandtl numbers $Pr = 0.7$ and 7. It is noted that for the case of $\xi = 0$ (pure forced convection), the $f''(0,0)$ value is 0.3321 for all values of Pr, n, and ϕ. It is also mentioned here that the results for $n = 0$ (the UWT case) have been given in ref. [16] only for $Pr = 0.7$ and 7 over the range of $0 \leqslant \xi \leqslant 10$. It can be seen from Figs. 1 and 2 that for a given value of the buoyancy force parameter ξ, the local friction factor decreases with an increase in the exponent n. On the other hand, the local Nusselt number increases with increasing value of the exponent n, Figs. 3 and 4. Also, a higher inclination angle ϕ gives rise to a larger friction factor and a larger Nusselt number.

In the numerical calculations for the flow instability, the buoyancy force parameter ξ was varied from 0.001 to 0.1 for all the inclination angles ϕ and exponent values n that were computed. This range of buoyancy force parameter covers Reynolds and Grashof numbers of practical interest in laminar boundary-layer flows. It is pointed out that vortex instability of the flow does not exist when the plate is vertical, because in this situation there is no normal buoyancy force component acting on the plate that is responsible for the vortex instability of the flow. To determine the stability and instability domains and to obtain the critical values of Gr_x, Re_x, and α for the onset of the vortex instability for various values of the exponent n, inclination angle ϕ, and buoyancy force parameter ξ, calculations were carried out for $Pr = 0.7$, 7, 100, and 1000.

Representative neutral stability curves (in the form of $Re_x^{1/2}$ vs α curves) for $Pr = 100$ and $\phi = 45^\circ$ are plotted in Fig. 5. This figure shows the effect of the buoyancy force parameter ξ on the neutral stability curves for various values of the exponent n. As expected, a larger buoyancy force parameter ξ will provide lower critical values of $Re_x^{1/2}$, i.e. a less stable flow. This same trend was also found in refs. [2, 3]. Also, an increase in the value of n is seen to give a larger critical $Re_x^{1/2}$ value, i.e. a more stable flow. Tables 1 and 2 list the minimum critical values of $Re_x^{*1/2}$ and the corresponding wave numbers α^* for different values of the exponent n, the inclination angle ϕ, and the buoyancy force parameter ξ for $Pr = 100$

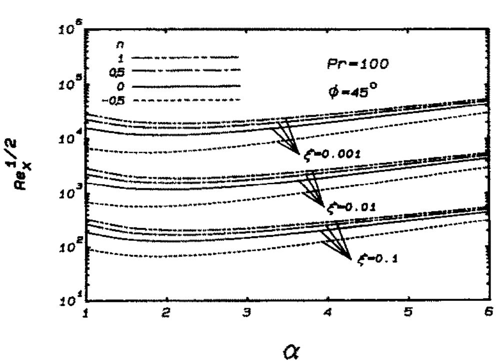

FIG. 5. The effect of buoyancy force parameter on the neutral stability curves for $Pr = 100$ and $\phi = 45^\circ$; $-0.5 \leqslant n \leqslant 1.0$.

and 1000, respectively. From these tables, one can see that a higher Prandtl number gives rise to a higher critical $Re_x^{*1/2}$ value (except $\xi = 0.1$) and a larger critical wave number α^*.

It is interesting to see the effect of the exponent n on the neutral stability curves $Gr_x/Re_x^{3/2}$ vs α for different inclination angles ϕ. This is shown in Figs. 6–8, respectively, for $Pr = 0.7$, 100, and 1000. To avoid crowding, only results for two inclination angles are shown in each figure. The results for $\phi = 0°$ (and $\xi = 0$) for $Pr = 100$ and 1000 are given in ref. [12] and are not shown here. It can be seen from these figures that as the exponent n increases, the neutral stability curve shifts upward to a larger value of $Gr_x/Re_x^{3/2}$. That is, the flow will become more stable to the vortex mode of instability as the exponent n increases. In addition, it can be observed that the larger the exponent n, the larger is the critical wave number α^* (corresponding to the minimum value of $Gr_x/Re_x^{3/2}$). However, the critical wave number appears to be unaffected by the inclination angle, which is in agreement with the experimental results of Sparrow and Husar [20]. This behavior can be best observed from Fig. 9 which is a representative α^* vs ϕ plot for $Pr = 100$.

The fact that the flow will become less susceptible to the vortex mode of instability as the value of n increases can be explained as follows: When $n = 0$ there is a step jump in the temperature difference $(T_w - T_\infty) = A$ for all x, whereas for $n > 0$ the wall temperature starts with $T_w = T_\infty$ at $x = 0$ and increases with x. For $n < 0$, it starts with $T_w \to \infty$ at $x = 0$ and decreases with increasing x. Thus, when $n < 0$ a larger jump in $(T_w - T_\infty)$ occurs at a smaller x location than when $n = 0$. This contributes to an earlier onset of the flow instability and hence a smaller critical value of $Gr_x/Re_x^{3/2}$. This same trend was also reported in the work of refs. [12, 13].

To determine the onset of the vortex instability, the minimum critical values of $Gr_x^*/Re_x^{*3/2}$, denoted by G^*, from the present calculations for different values of n are plotted in Figs. 10–13, respectively, for $Pr = 0.7$, 7, 100, and 1000 over the inclination angles $0° \leq \phi \leq 85°$. They are also listed in Table 3. It can be seen from these figures and the table that the critical $Gr_x^*/Re_x^{*3/2}$ value increases with increasing inclination angle ϕ (for a given Prandtl number) and with increasing Prandtl number (for a given angle of inclination ϕ). This implies that the flow becomes more stable to the vortex mode of instability as the plate is tilted toward the vertical orientation and that fluids with larger Prandtl numbers stabilize the flow.

As mentioned earlier, numerical difficulties were encountered in obtaining neutral stability curves and critical values of $Gr_x^*/Re_x^{*3/2}$ for $Pr = 0.7$ and 7 because of the relatively small critical wave number. However, inspection of Figs. 12 and 13 for $Pr = 100$ and 1000 reveals that the G^* vs ϕ curves are parallel

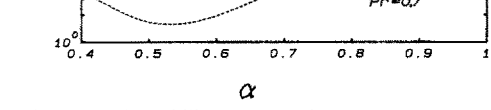

FIG. 6. Neutral stability curves for $Pr = 0.7$; $\phi = 0°$, $\phi = 85°$; $-0.5 \leq n \leq 1.0$.

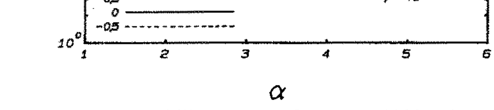

FIG. 8. Neutral stability curves for $Pr = 1000$; $\phi = 45°$, $\phi = 85°$; $-0.5 \leq n \leq 1.0$.

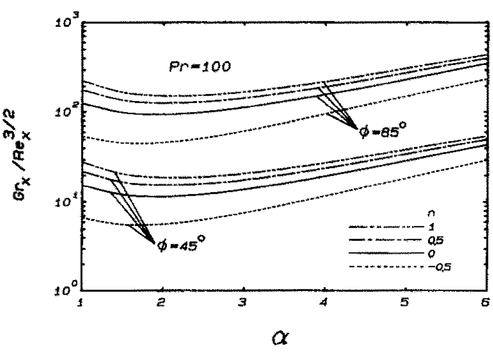

FIG. 7. Neutral stability curves for $Pr = 100$; $\phi = 45°$, $\phi = 85°$; $-0.5 \leq n \leq 1.0$.

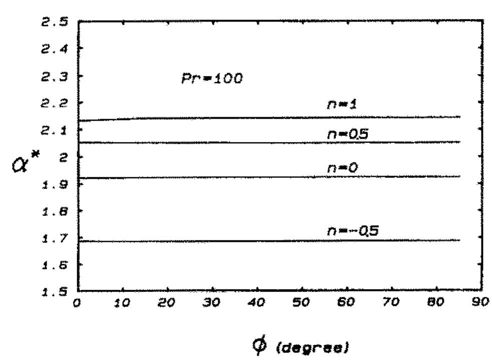

FIG. 9. The critical wave number α^* as a function of ϕ, $Pr = 100$.

Table 1. The minimum critical values of $Re_x^{*1/2}$ and α^* for $Pr = 100$

	$\phi = 15°$		$\phi = 30°$		$\phi = 45°$		$\phi = 60°$		$\phi = 75°$		$\phi = 85°$	
(ξ, n)	$Re_x^{*1/2}$	α^*	$Re_x^{*1/2}$	α^*	$Re_x^{*1/2}$	α^*	$Re_x^{*1/2}$	α^*	$Re_x^{*1/2}$	α^*	$Re_x^{*1/2}$	α^*
(0.001, 1)	13857	2.1418	15460	2.1429	18937	2.1431	26785	2.1437	51750	2.1439	153680	2.1448
(0.001, 0.5)	11418	2.0519	12740	2.0512	15606	2.0503	22075	2.0517	42649	2.0519	126650	2.0533
(0.001, 0)	8454.2	1.9256	9433.0	1.9259	11556	1.9265	16347	1.9270	31585	1.9269	93801	1.9268
(0.001, −0.5)	4063.9	1.6863	4536.5	1.6870	5559.9	1.6880	7867.1	1.6886	15203	1.6883	45153	1.6891
(0.01, 1)	1388.7	2.1440	1552.3	2.1462	1904.7	2.1482	2697.4	2.1510	5215.7	2.1514	15493	2.1514
(0.01, 0.5)	1144.8	2.0534	1280.2	2.0564	1571.5	2.0591	2226.3	2.0609	4305.5	2.0624	12790	2.0638
(0.01, 0)	848.40	1.9296	949.71	1.9336	1166.8	1.9362	1653.9	1.9396	3199.9	1.9413	9506.7	1.9416
(0.01, −0.5)	409.62	1.6948	460.56	1.7038	567.92	1.7108	807.33	1.7163	1564.6	1.7195	4651.0	1.7204
(0.1, 1)	141.65	2.1670	161.13	2.1921	200.57	2.2111	287.10	2.2249	558.75	2.2326	1663.0	2.2355
(0.1, 0.5)	117.26	2.0805	133.93	2.1077	167.24	2.1304	239.92	2.1463	467.59	2.1571	1392.2	2.1613
(0.1, 0)	87.655	1.9635	100.91	1.9952	128.81	2.0237	182.68	2.0391	356.97	2.0509	1063.6	2.0557
(0.1, −0.5)	43.905	1.7626	52.144	1.8168	67.010	1.8576	98.034	1.8863	193.24	1.9043	577.27	1.9092

Table 2. The minimum critical values of $Re_x^{*1/2}$ and α^* for $Pr = 1000$

	$\phi = 15°$		$\phi = 30°$		$\phi = 45°$		$\phi = 60°$		$\phi = 75°$		$\phi = 85°$	
(ξ, n)	$Re_x^{*1/2}$	α^*	$Re_x^{*1/2}$	α^*	$Re_x^{*1/2}$	α^*	$Re_x^{*1/2}$	α^*	$Re_x^{*1/2}$	α^*	$Re_x^{*1/2}$	α^*
(0.001, 1)	14091	4.6988	15718	4.6971	19252	4.6982	27228	4.7019	52603	4.7000	156210	4.6982
(0.001, 0.5)	11641	4.5234	12986	4.5243	15906	4.5247	22496	4.5217	43461	4.5259	129070	4.5243
(0.001, 0)	8659.3	4.2609	9660.0	4.2604	11833	4.2550	16736	4.2587	32334	4.2628	96020	4.2615
(0.001, −0.5)	4215.4	3.8058	4703.4	3.8072	5762.3	3.8074	8151.2	3.8082	15749	3.8058	46772	3.8090
(0.01, 1)	1410.5	4.7045	1574.8	4.7022	1930.4	4.7086	2731.9	4.7090	5279.8	4.7096	15681	4.7124
(0.01, 0.5)	1165.5	4.5230	1301.6	4.5256	1595.8	4.5391	2258.6	4.5322	4365.6	4.5338	12966	4.5344
(0.01, 0)	867.37	4.2629	969.08	4.2674	1188.6	4.2620	1682.8	4.2706	3253.3	4.2747	9663.0	4.2747
(0.01, −0.5)	423.08	3.8128	473.65	3.8213	581.97	3.8268	825.03	3.8316	1596.3	3.8309	4742.6	3.8349
(0.1, 1)	142.45	4.7220	160.47	4.7506	198.19	4.7678	282.08	4.7862	547.09	4.7975	1626.6	4.7975
(0.1, 0.5)	117.95	4.5495	133.15	4.5765	164.72	4.6056	234.73	4.6234	455.62	4.6322	1354.9	4.6358
(0.1, 0)	88.153	4.2978	99.931	4.3328	124.05	4.3677	177.22	4.3837	344.52	4.3985	1025.0	4.4018
(0.1, −0.5)	43.802	3.8742	50.524	3.9318	63.582	3.9842	91.719	4.0329	179.33	4.0509	534.46	4.0568

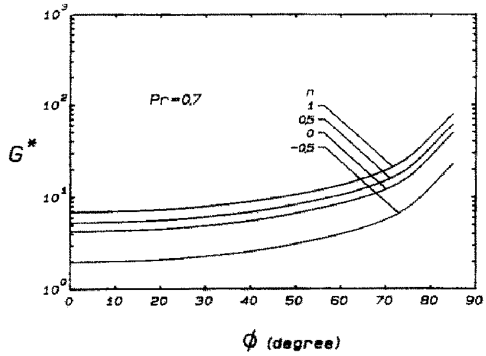

FIG. 10. The critical value $G^* = Gr_x^*/Re_x^{*3/2}$ as a function of ϕ, $Pr = 0.7$.

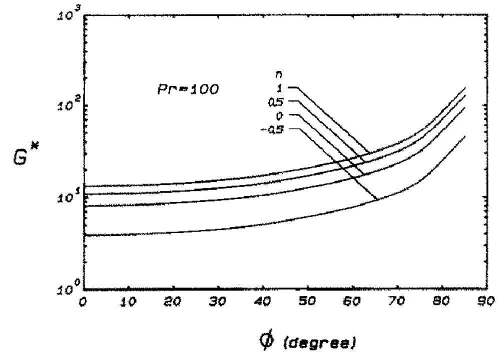

FIG. 12. The critical value $G^* = Gr_x^*/Re_x^{*3/2}$ as a function of ϕ, $Pr = 100$.

for all n values. This implies that for a given Prandtl number there exists a certain ratio between the G^* values for any two n values at a given ϕ. This same characteristic can also be found between two Prandtl numbers for given values of n and ϕ. Thus, if the G^* values are available at $\phi = 0$ and 85° for $Pr = 0.7$ and 7, the G^* values at other angles ϕ for these two Prandtl numbers can be obtained by an interpolation without the need for actual calculations. Table 4 shows the ratio of the critical values of $G^* = Gr_x^*/Re_x^{*3/2}$ for $Pr = 1000$ and 100 for different exponent values n at various angles of inclination. It can be seen from the table that for a given n value the G^* ratio between the two Prandtl numbers, $Pr = 1000$ and 100, is found to remain essentially constant for all angles of inclination. This means that with the G^* ratio for any two Prandtl numbers, say $Pr = 100$ and 0.7, known for a given n at two fixed angles ϕ, say $\phi = 0$ and 85°, one can find the G^* values for all other angles between $\phi = 0$ and 85° for $Pr = 0.7$ with the known G^* values for $Pr = 100$.

The G^* values for $Pr = 0.7$ and $\phi = 85°$ were calculated and found to be 85.503 for $n = 1$, 60.613 for $n = 0.5$, 49.310 for $n = 0$, and 22.461 for $n = -0.5$. Also, the G^* values for $\phi = 0°$ are, from ref. [12], 6.8730, 5.2959, 4.2556, and 1.9853 for $n = 1$, 0.5, 0, and -0.5 for $Pr = 0.7$. The G^* ratios for $Pr = 100$ and 0.7 at $\phi = 0°$ are then found to be 1.9467 for $n = 1$, 2.0822 for $n = 0.5$, 1.9182 for $n = 0$, and 1.9756 for $n = -0.5$, as compared with 1.9450 for $n = 1$, 2.0895 for $n = 0.5$, 1.9023 for $n = 0$, and 2.0103 for $n = -0.5$ at $\phi = 85°$. Thus, it can be concluded from this that the same $Gr_x^*/Re_x^{*3/2}$ ratio between two Prandtl numbers can be obtained for a given exponent n for all angles ϕ. With the availability of the G^* results for $Pr = 0.7$ and 7 at $\phi = 0°$ [12], and the calculated G^* results for the same two Prandtl numbers at $\phi = 85°$, Figs. 10 and 11 were constructed by employing the interpolation method, as described.

Figures 14 and 15 illustrate the critical Re_x^* vs Gr_x^* plots for various inclination angles, respectively, for $Pr = 0.7$ and 7. Results from experiments [4, 6–8] are also included for comparison. A comparison between the results from the present analysis and those of the parallel flow model [2, 3] indicates that an accounting of the streamwise dependence of the disturbance amplitude functions stabilizes the flow. The results for $\phi = 0°$ (i.e. the horizontal plate) are taken from ref. [12]. Each straight line for a given ϕ separates the stable region above the line from the unstable region below the line. Thus, any flow condition determined by any combination of Re_x and Gr_x that lies below a straight line represents an unstable main flow situation as regards the vortex mode of instability, whereas any combination of Re_x and Gr_x above the line represents a stable flow situation. Inspection of Figs. 14 and 15 reveals that for a given Reynolds number the flow is most susceptible to the vortex

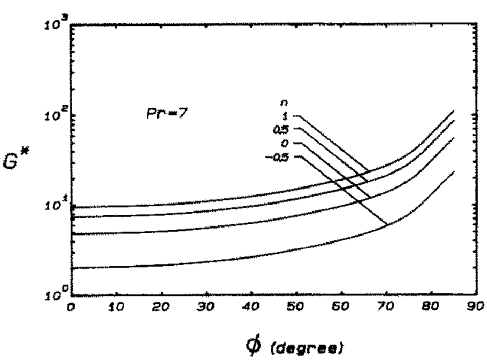

FIG. 11. The critical value $G^* = Gr_x^*/Re_x^{*3/2}$ as a function of ϕ, $Pr = 7$.

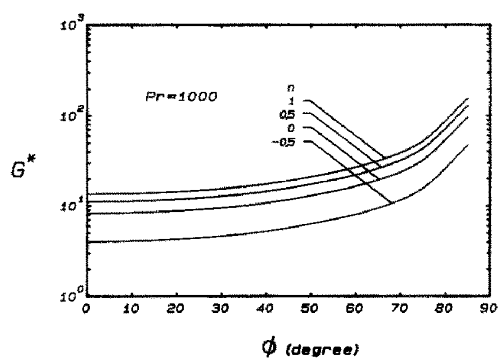

FIG. 13. The critical value $G^* = Gr_x^*/Re_x^{*3/2}$ as a function of ϕ, $Pr = 1000$.

Table 3. The minimum critical value of $G^* = Gr_x^*/Re_x^{*3/2}$

	$\phi = 0°$	$\phi = 30°$	$\phi = 45°$	$\phi = 60°$	$\phi = 75°$	$\phi = 85°$
(Pr, n)	$Gr_x^*/Re_x^{*3/2}$	$Gr_x^*/Re_x^{*3/2}$	$Gr_x^*/Re_x^{*3/2}$	$Gr_x^*/Re_x^{*3/2}$	$Gr_x^*/Re_x^{*3/2}$	$Gr_x^*/Re_x^{*3/2}$
(1000, 1)	13.609	15.718	19.252	27.228	52.603	156.21
(1000, 0.5)	11.243	12.986	15.906	22.496	43.461	129.07
(1000, 0)	8.3628	9.6600	11.833	16.736	32.334	96.020
(1000, −0.5)	4.0704	4.7034	5.7623	8.1512	15.749	46.772
(100, 1)	13.380	15.460	18.937	26.785	51.750	153.68
(100, 0.5)	11.027	12.740	15.606	22.075	42.649	126.65
(100, 0)	8.1631	9.4330	11.556	16.347	31.585	93.801
(100, −0.5)	3.9221	4.5365	5.5599	7.8671	15.203	45.153
(7, 1)	9.5394	11.022	13.501	19.097	36.896	109.57
(7, 0.5)	7.4243	8.5782	10.508	14.863	28.715	85.276
(7, 0)	4.8184	5.5673	6.8194	9.6460	18.636	55.344
(7, −0.5)	2.0241	2.3387	2.8647	4.0521	7.8287	23.249
(0.7, 1)	6.8730	7.9414	9.7285	13.578	26.583	78.942
(0.7, 0.5)	5.2959	6.1191	7.4954	10.602	20.483	60.828
(0.7, 0)	4.2556	4.9171	6.0230	8.5191	16.459	48.879
(0.7, −0.5)	1.9853	2.2939	2.8098	3.9743	7.6786	22.803

Table 4. The ratio of the minimum critical values $G^* = Gr_x^*/Re_x^{*3/2}$ for Pr = 1000 and 100

	$\phi = 15°$	$\phi = 30°$	$\phi = 45°$	$\phi = 60°$	$\phi = 75°$	$\phi = 85°$
n	$\frac{G^*_{Pr=1000}}{G^*_{Pr=100}}$	$\frac{G^*_{Pr=1000}}{G^*_{Pr=100}}$	$\frac{G^*_{Pr=1000}}{G^*_{Pr=100}}$	$\frac{G^*_{Pr=1000}}{G^*_{Pr=100}}$	$\frac{G^*_{Pr=1000}}{G^*_{Pr=100}}$	$\frac{G^*_{Pr=1000}}{G^*_{Pr=100}}$
1	1.0170	1.0170	1.0170	1.0170	1.0165	1.0165
0.5	1.0195	1.0193	1.0192	1.0191	1.0190	1.0191
0	1.0243	1.0241	1.0240	1.0238	1.0237	1.0237
−0.5	1.0373	1.0370	1.0364	1.0361	1.0359	1.0359

mode of instability when $\phi = 0°$, that is, when the plate is horizontal. This susceptibility to instability diminishes as ϕ increases, eventually attaining an absolutely stable condition when $\phi = 90°$ (i.e. when the plate is vertical). From Figs. 14 and 15, one can see that the results of the present analysis bring the predicted critical Re_x^* and Gr_x^* values closer to the experimental results for air [4, 7, 8] and for water [6], but large discrepancies in the results still exist between the theory and experiments. To remedy the discrepancy between the two sets of results, further analyses using different approaches, such as linear theory with time-dependent amplitude function or nonlinear theory, appear to be in order.

CONCLUSION

In this paper, thermal instability of mixed convection in laminar boundary-layer flow over horizontal and inclined flat plates with power-law variation in the surface temperature has been investigated analytically using the linear theory based on a nonparallel flow model. Neutral stability curves as well as critical Reynolds number, critical Grashof number,

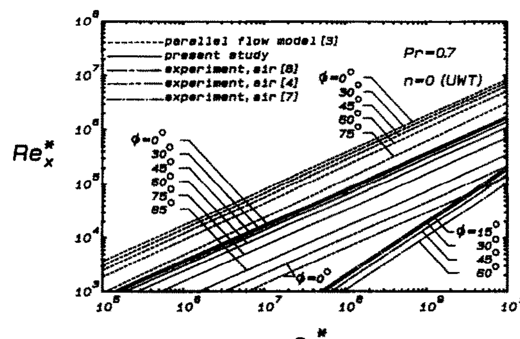

FIG. 14. Critical Reynolds number vs critical Grashof number for various inclination angles, Pr = 0.7.

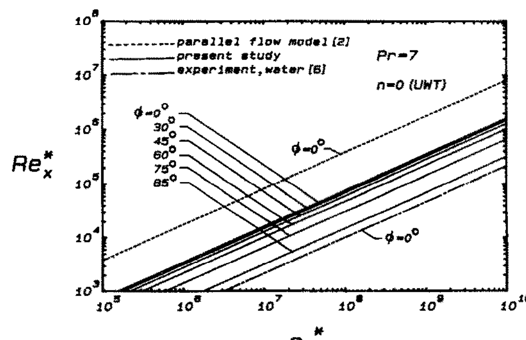

FIG. 15. Critical Reynolds number vs critical Grashof number for various inclination angles, Pr = 7.

and critical wave numbers are presented for Prandtl numbers of 0.7, 7, 100, and 1000, covering a range of exponent values $-0.5 \leqslant n \leqslant 1.0$ and inclination angles $0^\circ \leqslant \phi \leqslant 85^\circ$. The major findings from the present study are:

(1) For the power-law variation in the wall temperature, both the critical values of $Gr_x^*/Re_x^{*3/2}$ and wave number α^* increase with an increasing value of the exponent n for a given Prandtl number Pr or inclination angle ϕ.

(2) For a given value of the exponent n or Prandtl number Pr, the critical value of $Gr_x^*/Re_x^{*3/2}$ increases with increasing inclination angle ϕ. However, the critical wave number α^* appears to be unaffected by the inclination angle.

(3) The more rigorous analysis based on the nonparallel flow model in the present study provides a larger critical $Gr_x^*/Re_x^{*3/2}$ value than the previous analyses based on the parallel flow model, thus bringing the critical values closer to available experimental data.

REFERENCES

1. R. S. Wu and K. C. Cheng, Thermal instability of blasius flow along horizontal plates, *Int. J. Heat Mass Transfer* **19,** 907–913 (1976).
2. A. Moutsoglou, T. S. Chen and K. C. Cheng, Vortex instability of mixed convection flow over a horizontal flat plate, *J. Heat Transfer* **103,** 257–261 (1981).
3. T. S. Chen, A. Moutsoglou and B. F. Armaly, Thermal instability of mixed convection flow over inclined surfaces, *Numer. Heat Transfer* **5,** 343–352 (1982).
4. Y. Hayashi, A. Takimoto and K. Hori, Heat transfer in laminar mixed convection flow over a horizontal flat plate (in Japanese), *Proc. 14th Japan Heat Transfer Symp.*, pp. 4–6 (1977).
5. H. Imura, R. R. Gilpin and K. C. Cheng, An experimental investigation of heat transfer and buoyancy induced transition from laminar forced convection to turbulent free convection over a horizontal isothermally heat plate, *J. Heat Transfer* **100,** 429–434 (1978).
6. R. R. Gilpin, H. Imura and K. C. Cheng, Experiments on the onset of longitudinal vortices in horizontal blasius flow heated from below, *J. Heat Transfer* **100,** 71–77 (1978).
7. H. I. Abu-Mulaweh, B. F. Armaly and T. S. Chen, Instabilities of mixed convection flows adjacent to inclined plates, *J. Heat Transfer* **109,** 1031–1033 (1987).
8. S. S. Moharreri, B. F. Armaly and T. S. Chen, Measurements in the transition vortex flow regime of mixed convection above a horizontal heated plate, *J. Heat Transfer* **110,** 358–365 (1988).
9. K. C. Cheng, T. Obata and R. R. Glipin, Buoyancy effects on forced convection heat tansfer in the transition regime of a horizontal boundary layer heated from below, *J. Heat Transfer* **110,** 596–603 (1988).
10. K. Chen and M. M. Chen, Thermal instability of forced convection boundary layers, *J. Heat Transfer* **106,** 284–289 (1984).
11. J. Y. Yoo, P. Park, C. K. Choi and S. T. Ro, An analysis on the thermal instability of forced convection flow over isothermal horizontal flat plate, *Int. J. Heat Mass Transfer* **30,** 927–935 (1987).
12. H. R. Lee, T. S. Chen and B. F. Armaly, Nonparallel thermal instability of forced convection flow over a heated, nonisothermal horizontal flat plate, *Int. J. Heat Mass Transfer* **33,** 2019–2028 (1990).
13. H. R. Lee, T. S. Chen and B. F. Armaly, Nonparallel vortex instability of natural convection flow over a nonisothermal horizontal flat plate, *Int. J. Heat Mass Transfer* **34,** 305–313 (1991).
14. H. R. Lee, T. S. Chen and B. F. Armaly, Nonparallel thermal instability of natural convection flow on nonisothermal inclined flat plates, *Int. J. Heat Mass Transfer* **35,** 207–220 (1992).
15. S. L. Lee, T. S. Chen and B. F. Armaly, New finite difference solution methods for wave instability problems, *Numer. Heat Transfer* **10,** 1–18 (1986).
16. A. Mucoglu and T. S. Chen, Mixed convection on inclined surfaces, *J. Heat Transfer* **101,** 422–426 (1979).
17. S. E. Haaland and E. M. Sparrow, Vortex instability of natural convection flow on inclined surfaces, *Int. J. Heat Mass Transfer* **16,** 2355–2367 (1973).
18. C. T. Hsu, P. Cheng and G. M. Homsy, Instability of free convection flow over a horizontal impermeable surface in a porous medium, *Int. J. Heat Mass Transfer* **21,** 1221–1228 (1978).
19. C. T. Hsu and P. Cheng, Vortex instability in buoyancy-induced flow over inclined heated surfaces in porous media, *J. Heat Transfer* **101,** 660–665 (1979).
20. E. M. Sparrow and R. B. Husar, Longitudinal vortices in natural convection flow on inclined surfaces, *J. Fluid Mech.* **37,** 251–255 (1969).

INSTABILITE THERMIQUE NON PARALLELE DE LA CONVECTION MIXTE SUR DES PLAQUES PLANES NON ISOTHERMES, HORIZONTALES ET INCLINEES

Résumé—Une théorie linéaire basée sur un modèle d'écoulement non parallèle est utilisée pour étudier l'apparition de l'instabilité tourbillonnaire longitudinale de la convection mixte laminaire sur des plaques planes horizontales et inclinées avec température pariétale non uniforme $T_w(x) - T_\infty = Ax^n$. Dans cette analyse, on tient compte de la variation longitudinale de l'amplitude de la perturbation. Les courbes de stabilité neutre, les valeurs critiques du paramètre $G^* = Gr_x^*/Re_x^{*3/2}$ et du nombre d'onde α^* sont présentés pour des nombres de Prandtl $Pr = 0{,}7$, 7, 100 et 1000, un exposant n tel que $-0{,}5 \leqslant n \leqslant 1{,}0$ et un angle d'inclinaison $0^\circ \leqslant \phi \leqslant 85^\circ$. Pour un nombre de Prandtl et un angle d'inclinaison donnés, l'instabilité thermique diminue quand n augmente. Pour des valeurs données de n et de Pr, la valeur critique de G^* croît avec l'angle d'inclinaison. Le nombre d'onde critique α^* semble être indépendant de l'angle d'inclinaison. Les résultats de cette analyse sont comparés à ceux d'autres études analytiques et expérimentales. Selon l'étude faite, la dépendance de l'amplitude est trouvée avoir un effet stabilisant en comparaison avec le cas de l'analyse de l'écoulement parallèle qui néglige cette dépendance.

NICHTPARALLELE THERMISCHE INSTABILITÄT BEI MISCHKONVEKTION AN NICHTISOTHERMEN HORIZONTALEN UND GENEIGTEN EBENEN PLATTEN

Zusammenfassung—Eine lineare Theorie auf der Grundlage nichtparalleler Strömung wird bei der Untersuchung des Einsetzens der Längswirbelinstabilität bei laminarer Mischkonvektion an horizontalen und geneigten ebenen Platten mit variabler Oberflächentemperatur ($T_w(x) - T_\infty = A \cdot x^n$) zu untersuchen. Dabei wird eine strömungsabhängige Funktion der Störungsamplitude berücksichtigt. Kurven neutraler Stabilität sowie kritische Werte des Parameters $G^* = Gr_x^*/Re_x^{*3/2}$ und Wellenzahlen α^* werden für folgende Parameter vorgestellt: Prandtl-Zahl $Pr = 0{,}7$; 7; 100 und 1000, Exponenten n von $-0{,}5$ bis 1,0, Neigungswinkel $0° \leqslant \phi \leqslant 85°$. Für gegebene Werte der Prandtl-Zahl und des Neigungswinkels nimmt die thermische Instabilität mit steigenden Werten des Exponenten n ab. Bei gegebenen Werten des Exponenten n und der Prandtl-Zahl Pr nimmt der kritische Wert von $Gr_x^*/Re_x^{*3/2}$ mit zunehmendem Neigungswinkel gegenüber der Waagerechten zu. Die kritische Wellenzahl α^* jedoch scheint unabhängig vom Neigungswinkel zu sein. Die Ergebnisse aus der hier vorgestellten Untersuchung mit nichtparalleler Strömung wird mit verfügbaren analytischen und experimentellen Ergebnissen verglichen. Wird die strömungsabhängige Amplitudenfunktion bei der nicht-parallelen Strömungsanalyse berücksichtigt, so bedingt dies einen Stabilisierungseffekt gegenüber Modellen, welche diese Abhängigkeit nicht berücksichtigen.

ТЕПЛОВАЯ НЕУСТОЙЧИВОСТЬ НЕПАРАЛЛЕЛЬНОГО ТЕЧЕНИЯ ПРИ СМЕШАННОЙ КОНВЕКЦИИ НА НЕИЗОТЕРМИЧЕСКИХ ГОРИЗОНТАЛЬНОЙ И НАКЛОННОЙ ПЛОСКИХ ПЛАСТИНАХ

Аннотация—Линейная теория на основе модели непараллельных течений используется для исследования возникновения продольной вихревой неустойчивости ламинарного потока при смешанной конвекции, обтекающего горизонтальную и наклонную плоские пластины с температурой поверхности, изменяющейся по закону $T_w(x) - T_\infty = Ax^n$. В анализе учитывается неоднородность по потоку амплитудных функций возмущения. Приводятся нейтральные кривые устойчивости, а также критические значения параметра $G^* = Gr_x^*/Re_x^{*3/2}$ и волновые числа α^* для чисел Прандтля $Pr = 0{,}7$; 7; 100 и 1000 в интервале значений показателя степени $-0{,}5 \leqslant n \leqslant 1{,}0$ и углов наклона $0° \leqslant \phi \leqslant 85°$. При заданных числе Прандтля и угле наклона найдено, что неустойчивость уменьшается с ростом значения n. Кроме того, при указанных значениях показателя степени n и числе Прандтля Pr критическое значение $Gr_x^*/Re_x^{*3/2}$ возрастает с увеличением угла наклона относительно горизонтали. Однако оказалось, что критическое волновое число α^* не зависит от угла наклона. Результаты проведенного анализа сравниваются с имеющимися аналитическими и экспериментальными данными предыдущих исследований. Анализ показал, что непараллельные течения при учете неоднородности амплитудных функций в потоке оказывают стабилизирующее влияние в отличие от параллельного течения в пренебрежении этой зависимостью.